Progress In Electromagnetics Research M, Vol. 10, 103–117, 2009

ANALYSIS OF COMPLEX ANTENNA AROUND ELECTRICALLY LARGE PLATFORM USING ITERATIVE VECTOR FIELDS AND UTD METHOD

Z. L. He, K. Huang, and C. H. Liang

National Key Laboratory of Antennas and Microwave Technology
Xidian University
Xi'an 710071, China

Abstract—A new efficient technique for the analysis of complex antenna around a scatterer is proposed in this paper, termed the iterative vector fields with uniform geometrical theory of diffraction (UTD) technique. The complex field vector components on the closed surface enclosing the antenna without platform are computed by higher order Method of Moments (MOM), and the scattered fields from the platform are calculated by UTD method. The process of iteration is implemented according to the equivalence theorem. Based on this approach, an approximation method is outlined, in which the computational time is saved largely, while the accuracy is not reduced. The relative patterns obtained from the present method and the approximation method both show good agreements with that obtained from MOM.

1. INTRODUCTION

Numerical techniques for calculation of electromagnetic fields can be favorably divided into accurate methods and high-frequency or asymptotic methods. Accurate methods are high in precision, but the requirements of computational resource increase greatly with the scale of mesh especially in solving electrically large problems. High-frequency method [1] is widely used to solve electrically large problems, but the accuracy is not satisfying. It is well-known that hybridization of two-field calculation techniques belonging to different groups [2–5] has great potential to increase the capabilities of the individual

Corresponding author: Z.-L. He (hzl020314@126.com).

methods. Actually many hybrid methods have emerged. The iterative MOM-PO (Physical-optics) technique was proposed to analyze the antenna around NURBS surface [5], while it has not been applied to analyze complex antenna. Hybrid FDTD/UTD was applied to analyze phased array antennas mounted on airborne platform in [6]. Combining UTD with MOM was used to calculate the pattern of the antenna in complex environment in [7]. The effect of platform on the current distribution on antenna has been neglected in [6, 7] supposing that antenna is far away from the platform. It's obvious that the methods are decoupled. And the hybrid MOM-PO method based parallel was proposed in [8] to deduce the computational time. Commercial software HOBIES [9–11] (Higher-order Basis functions based Integral Equation Solver), is a general purpose Frequency Domain Electromagnetic integral equation solver. HOBIES provides solutions based on MoM employing higher order basis functions. The use of higher order basis functions substantially reduces the number of unknowns, reducing the problem size and hence the total solution time [12]. Even if the efficiency has been enhanced, it needs unbearable hardware requirements in solving electronically large problems. When analyzing EMC problems of electrically large platforms, UTD [13, 14] method is widely used and reasonably effective. Based on ray solutions, UTD is an efficient high-frequency method, which is utilized to calculate the scattered field from electrically large platform in this paper.

In this paper, an iterative vector fields and UTD method is presented to analyze the radiation pattern of complex antenna around electrically large platform. We consider full coupling between antenna and platform through iterating Huygens' surface currents instead of the conventional MOM-UTD process of modifying the impedance matrix of MoM with UTD. The results obtained from the present method and the approximation method both show good agreements with that obtained from MOM, which shows the validity and accuracy of this approach.

2. HIGHER ORDER MOM (HOBIES)

Commercial software HOBIES solves the integral equation utilizing higher order MoM. As the name suggests, higher order MOM uses both higher order geometric surfaces and higher order basis functions [12, 15].

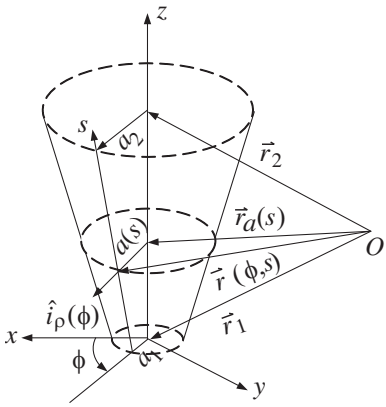

Figure 1. A truncated cone.

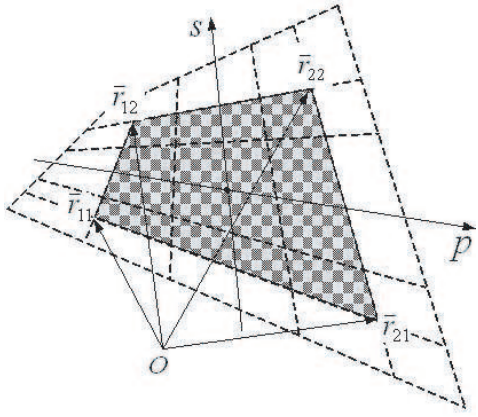

Figure 2. Bilinear patch defined by four position vectors and vertices.

2.1. Higher Order Surfaces

A right-truncated cone is determined by position vectors $\vec{r}_1$, $\vec{r}_2$ and the radii of its beginning and end a_1, a_2, as shown in Fig. 1. Generalized wires can be approximated by right-truncated cones. The parametric equation of the cone surface can be written as

$$\vec{r}_a(\phi, s) = \vec{r}_a(s) + a(s)\,\hat{i}_\rho(\phi), \quad -1 \le s \le 1, \quad -\pi \le \phi \le \pi \qquad (1)$$

where ϕ and s are parameters of the cone surface, ϕ is the circumferential angle, measured from the x-axis, s is measured along generatrix from the beginning to the end, and $\hat{i}_\rho(\phi)$ is the radial unit vector perpendicular to the cone axis.

Bilinear surface is applied in commercial software HOBIES. The two parameters of which a bilinear surface consists are p and s-components, as shown in Fig. 2. The parametric equation of such an isoparametric element can be written in the following form:

$$\begin{aligned}\vec{r}(p,s) \;=\; & \vec{r}_{11}\frac{(1-p)(1-s)}{4} + \vec{r}_{12}\frac{(1-p)(1+s)}{4} + \vec{r}_{21}\frac{(1+p)(1-s)}{4} \\ & + \vec{r}_{22}\frac{(1+p)(1+s)}{4}, \quad -1 \le p \le 1, \quad -1 \le s \le 1 \end{aligned} \qquad (2)$$

where $\vec{r}_{11}, \vec{r}_{12}, \vec{r}_{21}$ and $\vec{r}_{22}$ are the position vectors of its vertices, and p and s are the local coordinates.

2.2. Higher Order Basis Functions

Currents along wires are approximated by polynomials and can be written as

$$I(s) = I_1 N(s) + I_2 N(-s) + \sum_{i=2}^{N_s} a_i S_i(s) \tag{3}$$

where node basis function $N(s)$ and segment basis functions $S_j(s)$, $(i = 2, 4, \ldots N_s)$ are expressed as

$$N(s) = \frac{1-s}{2}, \quad S_i(s) = \begin{cases} s^i - 1, & i \text{ is even} \\ s^i - s, & i \text{ is odd} \end{cases} \tag{4}$$

respectively. a_i $(i = 2, 4, \ldots N_s)$ are the coefficients, and I_1, I_2 are the values of the currents at two wire ends, respectively.

The surface current over a bilinear surface is decomposed into its p and s-components, which is expressed as:

$$\vec{J}_s = J_{ss}\hat{s} + J_{sp}\hat{p} \tag{5}$$

The p-current component can be treated as the s-current component defined over the same bilinear surface with an interchange of the p and s coordinates. The approximations for the s-components of the electric and magnetic currents over a bilinear surface are typically defined by:

$$J_{ss}(p,s)\,\hat{s} \approx \sum_{i=0}^{N_p} \left[C_{i1}\vec{E}_i(p,s) + C_{i2}\vec{E}_i(p,-s) + \sum_{j=2}^{N_s} a_{ij}\vec{P}_{ij}(p,s) \right] \tag{6}$$

where C_{i1} and C_{i2} $(i = 0, 1, 2, \ldots N_p)$ are respectively defined by

$$C_{i1} = \sum_{j=0}^{N_s} a_{ij}(-1)^j, \quad C_{i2} = \sum_{j=0}^{N_s} a_{ij} \tag{7}$$

The edge basis functions $\vec{E}_i(p,s)$ and the patch basis functions $\vec{P}_{ij}(p,s)$ $(i = 0, 1, 2, \ldots N_p)$, $(j = 2, 4, \ldots N_s)$ are expressed as

$$\begin{aligned} \vec{E}_i(p,s) &= \frac{\frac{\partial \vec{r}(p,s)}{\partial s}}{\left| \frac{\partial \vec{r}(p,s)}{\partial p} \times \frac{\partial \vec{r}(p,s)}{\partial s} \right|} p^i N(s), \\ \vec{P}_{ij}(p,s) &= \frac{\frac{\partial \vec{r}(p,s)}{\partial s}}{\left| \frac{\partial \vec{r}(p,s)}{\partial p} \times \frac{\partial \vec{r}(p,s)}{\partial s} \right|} p^i S_j(s) \end{aligned} \tag{8}$$

The detailed presentation and discussion of $\vec{E}_i(p,s)$ and $\vec{P}_{ij}(p,s)$ can be found from Equations (16)–(19) in Section 3 of Ref. [15].

3. CALCULATION OF THE REFLECTED AND DIFFRACTED ELECTROMAGNETIC FIELDS BY UTD METHOD

Supposing the incidence fields are known, the formulas for reflected and diffracted electromagnetic fields in UTD method are given as follows.

Decompose the incidence fields into two components:

$$\begin{cases} \vec{E}^{\,i} = \hat{e}^i_{//} E^i_{//} + \hat{e}^i_{\perp} E^i_{\perp} \\ \vec{H}^{\,i} = \hat{e}^i_{//} H^i_{\perp} + \hat{e}^i_{\perp} H^i_{//} \end{cases} \tag{9}$$

where the unit vector perpendicular to the plane of incidence is denoted by $\hat{e}^i_{\perp}$, and the parallel by $\hat{e}^i_{//}$. $E^i_{//}$, $H^i_{//}$ are the components parallel to the plane of incidence, and $E^i_{\perp}$, $H^i_{\perp}$ are the ones perpendicular to the plane.

The reflected fields can be expressed as:

$$\begin{cases} \vec{E}^{\,r}\left(\vec{r}\right) \sim \vec{E}^{\,i}\left(Q_R\right) \cdot \overline{\overline{R}} \sqrt{\frac{\rho^r_1 \rho^r_2}{\left(\rho^r_1 + s^r\right)\left(\rho^r_2 + s^r\right)}} e^{-jks^r} \\ \vec{H}^{\,r}\left(\vec{r}\right) \sim \vec{H}^{\,i}\left(Q_R\right) \cdot \overline{\overline{R}} \sqrt{\frac{\rho^r_1 \rho^r_2}{\left(\rho^r_1 + s^r\right)\left(\rho^r_2 + s^r\right)}} e^{-jks^r} \end{cases} \tag{10}$$

where Q_R stands for the reflection point, ρ^r_1, ρ^r_2 are the principal radii of curvatures of reflected wavefront surface at Q_R, s^r is the distance along the reflected ray from Q_R to field point, and k is the wavenumber in given medium, $\vec{r}$ is the field point vector. The expression of $\overline{\overline{R}}$, dyadic reflection coefficient, is

$$\overline{\overline{R}} = R_s \hat{e}^i_{\perp} \hat{e}^r_{\perp} + R_h \hat{e}^i_{//} \hat{e}^r_{//} \tag{11}$$

in which the unit vector perpendicular to the plane of reflection is denoted by $\hat{e}^r_{\perp}$, the parallel by $\hat{e}^r_{//}$, and R_s, R_h are the soft and hard reflection coefficients.

The diffracted fields are denoted as:

$$\begin{cases} \vec{E}^{\,d}\left(\vec{r}\right) \sim \vec{E}^{\,i}\left(Q_E\right) \cdot \overline{\overline{D}} A\left(s, s^d\right) e^{-jks^d} \\ \vec{H}^{\,d}\left(\vec{r}\right) \sim \vec{H}^{\,i}\left(Q_E\right) \cdot \overline{\overline{D}} A\left(s, s^d\right) e^{-jks^d} \end{cases} \tag{12}$$

where Q_E is the point of diffraction, that is determined using the generalized Fermat's principle, $A(s, s^d)$ is the spatial attenuation factor depending on s^d and the local nature of the diffracting surface at Q_E, s means the distance between source point and Q_E, and s^d is the distance from Q_E to observation point, e^{-jks} is the phase factor. The dyadic diffraction coefficient, $\overline{\overline{D}}$ can be expressed as the sum of two dyads

$$\overline{\overline{D}} = -D_s \hat{e}^i_{\perp} \hat{e}^d_{\perp} - D_h \hat{e}^i_{//} \hat{e}^d_{//} \tag{13}$$

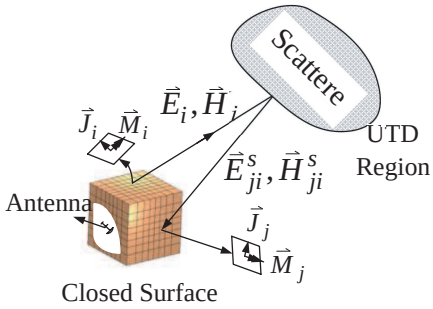

Figure 3. Modal of iteration.

where the unit vector perpendicular to the plane of diffraction is denoted by $\hat{e}_{\perp}^{d}$, the parallel by $\hat{e}_{//}^{d}$, and D_s, D_h are the soft and hard diffraction coefficients.

For any observation point $\vec{r}$ in lit region, the total scattered fields are:

$$\vec{E}_s\left(\vec{r}\right) = \vec{E}^{r}\left(\vec{r}\right) + \vec{E}^{d}\left(\vec{r}\right), \text{ and } \vec{H}_s\left(\vec{r}\right) = \vec{H}^{r}\left(\vec{r}\right) + \vec{H}^{d}\left(\vec{r}\right) \quad (14)$$

while in dark region

$$\vec{E}_s\left(\vec{r}\right) = \vec{E}^{d}\left(\vec{r}\right), \text{ and } \vec{H}_s\left(\vec{r}\right) = \vec{H}^{d}\left(\vec{r}\right). \quad (15)$$

Whether smooth convex surface or wedge, the above equations are applicable. The expressions of R_s, R_h and D_s, D_h can be obtained from references [13, 14].

4. MODIFYING THE ELECTRIC AND MAGNETIC CURRENTS OVER THE CLOSED SURFACE

Antenna is set as the MOM region and the platform as the UTD region in present approach. The system composed of platform and antenna will undergo a short-lived interaction when the latter is motivated. As shown in Fig. 3, the antenna practically motivated is enclosed by a closed surface S. The action of platform on antenna is transferred to the equivalent surface currents on S.

1). According to the equivalence theorem, determination of total electromagnetic field inside and outside S can be decomposed into two parts which can be analyzed separately. When the field outside surface S is considered, the field inside S equals to zero. To maintain the radiation of antenna outside S, it's necessary to induce electric and magnetic currents $\vec{J}_s$ and $\vec{M}_s$ in order to satisfy the continuity

condition of the field. The field outside S is uniquely determined by sources outside S and the equivalent currents placed on it, whose expressions are:

$$\vec{M}_S = \vec{E} \times \hat{n}, \quad \vec{J}_S = \hat{n} \times \vec{H} \tag{16}$$

where $\hat{n}$ is the outward unit normal vector on S, $\vec{E}$ and $\vec{H}$ are the fields on S produced by antenna without platform. Taking the electromagnetic field outside S as the research target, the antenna can be replaced by the currents placed on S. Once $\vec{J}_s$ and $\vec{M}_s$ are obtained, the antenna can be considered inexistent. The action of the platform on the antenna is transferred on the equivalent currents. So the method avoids the general process of modifying the MoM impedance matrix.

Theoretically, arbitrary shape closed surface can be used as S. For mathematical tractability, a cube is selected. Its six plane surfaces are all uniformly divided into small squares numbered with $1, 2 \ldots N$. The side length of a square is about $1/10\lambda$. The center of the ith square is regard as the ith sampling point (SP), at which the field produced by antenna without platform can be obtained by HOBIES, denoted by $\vec{E}_i^{Dir}$ and $\vec{H}_i^{Dir}$, where the superscript *Dir* represents the direct field, and the subscript i stands for the ith SP. Thus, the initial currents at the ith SP are:

$$\vec{M}_{Si}(0) = \vec{E}_i^{Dir} \times \hat{n}, \quad \vec{J}_{Si}(0) = \hat{n} \times \vec{H}_i^{Dir} \tag{17}$$

2) It is well known that the vector potential is:

$$\vec{A}(\vec{r}) = \frac{\mu}{4\pi} \iint\limits_S \vec{J}(\vec{r}') \frac{e^{-jkR}}{R} ds' \tag{18}$$

where R means the distance between the source location $\vec{r}'$ and observation point $\vec{r}$, S is the source region. According to the definition of $\vec{A}(\vec{r})$: $\nabla \times \vec{A} = \vec{B}$, the magnetic field produced by electric current density $\vec{J}(\vec{r}')$ over region S is:

$$\vec{H}_J(\vec{r}) = \frac{1}{4\pi} \iint\limits_S \left(\frac{1 + jkR}{R^3} \right) e^{-jkR} \left[\vec{J}(\vec{r}') \times \vec{R} \right] ds' \tag{19}$$

where the superscript J represents the field produced by electric currents. Then substituting Equation (19) into Maxwell equation $\nabla \times \vec{H} = j\omega\varepsilon\vec{E}$, the electric field produced by electric currents is

obtained through several simply algebraic steps:

$$\vec{E}_J = \frac{-j}{4\pi\omega\varepsilon}\iint\limits_S \left\{\frac{k^2R^2-3jkR-3}{R^5}e^{-jkR}\left\{\vec{R}\times\left[\vec{J}\left(\vec{r}'\right)\times\vec{R}\right]\right\} + \left(\frac{1+jkR}{R^3}\right)e^{-jkR}\cdot 2\vec{J}\left(\vec{r}'\right)\right\}ds' \tag{20}$$

where ω is angular frequency, ε is permittivity. The electric field produced by magnetic currents can be obtained by Equation (19) according to the dual theorem. In this case, sampling interval is so small that both the electric and magnetic currents distributing over an element are approximately thought uniform, which are equal to the currents on its center. Therefore, electric field produced by the ith surface element is approximated to:

$$\vec{E}_i\left(\vec{r}\right) \approx \frac{je^{-jkR_{i0}}\Delta s}{4\pi\omega\varepsilon}\cdot\left\{\frac{k^2R_{i0}^2-3jkR_{i0}-3}{R_{i0}^5}\cdot\left[\vec{J}_{si}\times\vec{R}_{i0}\times\vec{R}_{i0}\right] -2\vec{J}_{si}\cdot\left[\frac{1+jkR_{i0}}{R_{i0}^3}\right]\right\} - \frac{\Delta s}{4\pi}\left\{\frac{1+jkR_{i0}}{R_{i0}^3}e^{-jkR_{i0}}\left[\vec{M}_{si}\times\vec{R}_{i0}\right]\right\} \tag{21}$$

where Δs is the area of a small square, $\vec{R}_{i0}$ is the vector from the ith SP to the observation point, and $R_{i0} = |\vec{R}_{i0}|$. According to the dual theorem, relevant magnetic field vector can be deduced easily.

3) The ith SP is taken as the source point of UTD region, and the jth one as observation point, the scattered fields denoted as $\vec{E}^s_{ji}$ and $\vec{H}^s_{ji}$ are computed according to the UTD algorithm, where the superscript s represents the scattered field. For any $j \in [1, N]$, sum vectors $\vec{E}^s_j = \sum\limits_{i=1}^{N}\vec{E}^s_{ji}$, $\vec{H}^s_j = \sum\limits_{i=1}^{N}\vec{H}^s_{ji}$ are the total scattered field vectors at the jth SP. To maintain the field inside S be zero, it's necessary to induce new currents:

$$\Delta\vec{M}_{Sj} = \vec{E}^s_j\times(-\hat{n}), \quad \Delta\vec{J}_{Sj} = (-\hat{n})\times\vec{H}^s_j \tag{22}$$

$\vec{J}_{Sj}(k), \vec{M}_{Sj}(k)$ are supposed as the currents at the jth SP after the kth iteration, the ones after the $k+1$th iteration will be:

$$\begin{cases}\vec{M}_{Sj}(k+1) = \vec{M}_{Sj}(k) + \vec{E}^s_{j(k)}\times(-\hat{n}) \\ \vec{J}_{Sj}(k+1) = \vec{J}_{Sj}(k) + (-\hat{n})\times\vec{H}^s_{j(k)}\end{cases} \tag{23}$$

in which $\vec{E}^s_{j(k)}$ and $\vec{H}^s_{j(k)}$ stand for the vectors produced by the currents after the kth iteration. When the new currents are obtained, repeat

steps 2) and 3) until the conditions:

$$\frac{\left\|\vec{J}_s\left(k+1\right)-\vec{J}_s\left(k\right)\right\|}{\left\|\vec{J}_s\left(k\right)\right\|}\leq\Delta,\quad \frac{\left\|\vec{M}_s\left(k+1\right)-\vec{M}_s\left(k\right)\right\|}{\left\|\vec{M}_s\left(k\right)\right\|}\leq\Delta \tag{24}$$

are satisfied, where Δ is the threshold of iteration-ceasing, which is set as 10^{-5} in this paper, $\|\cdot\|$ denotes the 2-norm of a complex vector.

4) After the iteration cuts-off, taking the final currents on each SP as point sources, calculate the total scattered field at the observation point in far field region according to UTD algorithm. Adding the scattered field and the direct field without being sheltered, the total field can be obtained.

For saving computational time, we suppose the rays are emitted from the center of the cube because of its centre-symmetry. Thus for each observation point, reflection ray-tracing and shelter-judgment are respectively implemented only once, so does the diffraction case. The incidence field is precise, i.e., the summation of fields produced by each element. Based on this approximation, the computational time is reduced greatly, while the results are satisfying, which can be confirmed in Section 5.

5. NUMERICAL RESULTS AND ANALYSIS

In this section, all the examples are solved on a PC having a Pentium P4 3.0 GHz CPU, 1.0 GB RAM, and a 32-bit operating system called Microsoft Windows XP SP2.

5.1. Monopole Antenna Placed on a Pentagonal Plate with a Cylinder

As shown in Fig. 4, a monopole antenna toward $(0, 0, 1)$ is placed on a pentagonal plate with a frequency of 300 MHz, whose dimensional extensions are: $x : [-0.286, 0.354]$, $y : [-0.336, 0.336]$ and $z : [0.0, 0.25]$. The length of the monopole is $\lambda/4$. Closed surface is chosen as the cube centered at the origin, whose length of side is 0.90 m (0.9λ). The two centers of base surfaces of the cylinder scatterer are $(4.0, -3.0, -3.0)$, $(4.0, -3.0, 3.0)$, and the radii of which is 2 m. The six surfaces of the cube are all divided into 9×9 small squares. By six iterations, the final results of radiation pattern of the *xoy* plane and the *yoz* plane are shown in Figs. 5(a) and (b), both agree very well with the ones obtained by MOM.

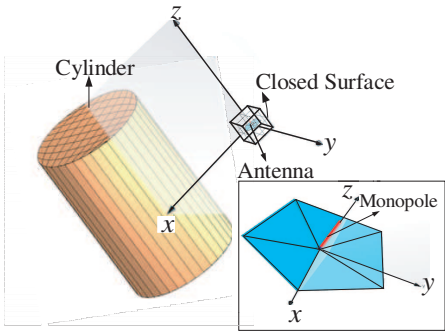

Figure 4. Monopole antenna placed on a pentagonal plate with a cylinder.

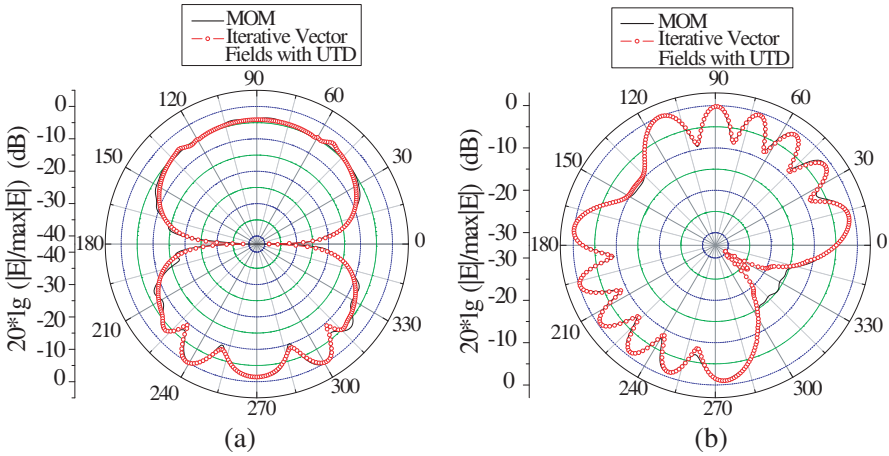

Figure 5. Results of radiation from monopole on a pentagonal plate near a cylinder. (a) Radiation pattern of the *xoy* plane. (b) Radiation pattern of the *yoz* plane.

5.2. LDPA with a Plate

The structure of Log-periodical dipole antenna (LDPA) with the working frequency of 700 MHz is shown in the inset of Fig. 6. Its three dimensional bounds are: $x : [0.139467, 0.7325]$, $y : [-0.25, 0.25]$, $z : [-0.02, 0.02]$ (m). A cube centered at $(0.4, 0, 0)$, whose side length is 0.8 m, is chosen as the closed surface. Its six plane surfaces are all divided into 20×20 small squares. The plate is centered at $(-5, 0, 0)$, whose sizes are shown in Fig. 6. It is placed parallel to the *yoz*

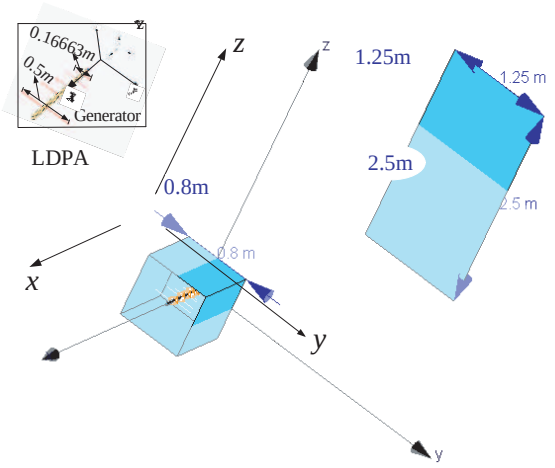

Figure 6. LDPA near a plate scatterer.

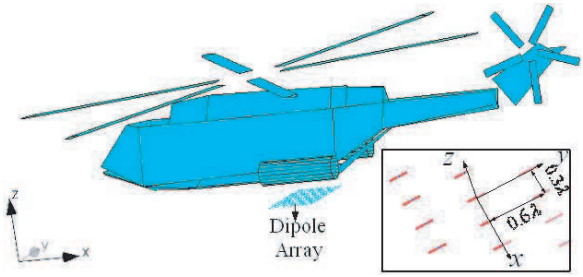

Figure 7. The modal of the airborne dipole phased array.

plane. Whether rigorous ray-tracing method or center ray-tracing approximation method, convergent solution can be obtained by five iterations in this example. It is worth noting that the two methods both converge in a few iterations.

The final results of radiation pattern in *xoy* and *yoz* plane by two iterative approaches, rigorous ray-tracing and approximate center ray-tracing, both agree very well with the ones obtained by higher order MOM shown in Figs. 8(a) and (b). In the *yoz* plane, the results within 258°−268° and 272°−282° are not accurate, and the most error is 3.6 dB. And the computing time respectively are 11258 seconds and 389 seconds. It's obviously to see that, comparing to the rigorous ray-tracing method, the center ray-tracing approximate method uses much less computational time, while the results are satisfying.

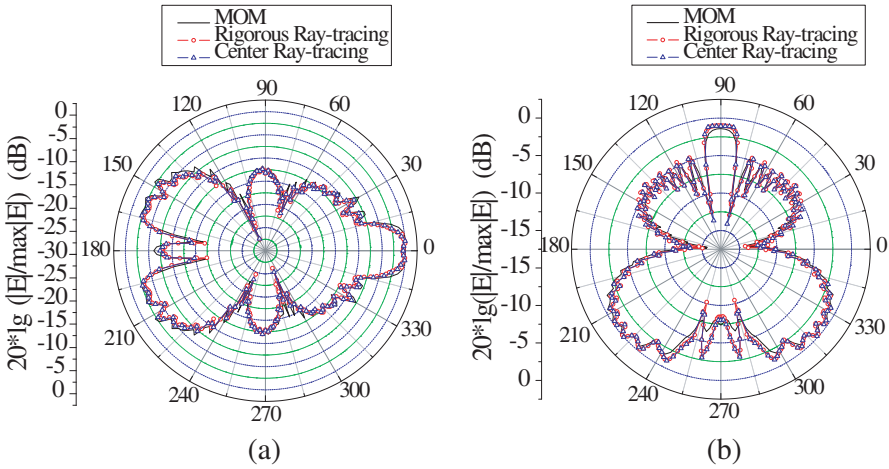

Figure 8. Results of radiation from LDPA near a plate. (a) Radiation pattern of the xoy plane. (b) Radiation pattern of the yoz plane.

5.3. Analysis of the Airborne Phase Array Antenna

The dipole array described in Ref. [16] is located below an airplane in the distance of 5λ, with the working frequency 2.0 GHz, as shown in Fig. 7. The local modal of the dipole array is shown in the inset of Fig. 7. We consider a 41×41 thin (radius equals 0.01λ), short (length amount to 0.2λ) and $\hat{y}$-directed dipole array, whose elements are phased to radiate a beam maximum in the direction of $(\theta = 60^\circ, \varphi = 45^\circ)$. The array has a period of 0.3λ and 0.6λ in x and y coordinates respectively, and is excited uniformly in amplitude. The total length of the airframe is 22.974m (about 153.16λ). A cube whose side length is 3.75 m is chosen as the closed surface, the center of which is located at the point $(0, 0, -3.5)$ under global coordinate. Its six plane surfaces are all divided into 250×250 small squares uniformly.

The convergent solutions are obtained by four iterations. The three-dimensional gain (dB) pattern is given in Fig. 9(a) and the normalized disturbed pattern of the airborne phase array is shown in (b). The disturbed pattern is calculated by the approximate center ray-tracing method. Because of the disturbance of airplane, the pattern changes largely. Obviously, the field above the airplane becomes smaller as a result of the shelter and reflection from airframe and airfoil, while below the plane strengthened. The radiation pattern of the complex antenna around electrically large platform can be effectively calculated using present method.

Figure 9. (a) Gain pattern of the dipole array (dB). (b) The normalized disturbed radiation pattern of the airborne phase array antenna.

From the examples above, we can see that both the rigorous ray-tracing method and center ray-tracing approximate method convergence in a few iterating times. It seems that the smaller the electrical distance between platform and surface, the stronger the scattered fields produced by the platform, so the greater the influence to the equivalent currents and more iterating times that needed to reach the convergence. However, the problem is complex in practice. The iterating times should be dependent on not only the distance between antenna and platform but also the radiation direction, the electric size of the scatterer, the posture of the antenna relative to the scatterer etc. Therefore, such a conclusion should be futher studied.

6. CONCLUSION

This paper has proposed an iterative method, which employs HOBIES to compute complex field vector components over the closed surface near the antenna without platform, and iteriates the equivalent electric and magnetic currents by UTD method. Since the ray-tracing of UTD method is time-consuming, the paper has presented an approximate method. Three examples are given, and the results obtained from present methods and from pure MoM approach agree very well. The examples have demonstrated the advantages of this method over the commonly hybrid methods, especially when the antenna is complex. Considering the action of platform on the currents distribution along

antenna, the results are more appropriate than the ones obtained in references [6, 7]. The approach presented in this paper might be very useful in practical engineering.

REFERENCES

1. Li, X.-F., Y.-J. Xie, and R. Yang, "High-frequency method analysis on scattering from homogenous dielectric objects with electrically large size in half space," *Progress In Electromagnetics Research B*, Vol. 1, 177–178, 2008.
2. Thiele, G. and T. Newhouse, "A hybrid technique for combining moment methods with the geometrical theory of diffraction," *IEEE Trans. Antennas Propagat.*, Vol. 23, No. 1, 62–69, 1975.
3. Zhang, P.-F., S.-X. Gong, and S.-F. Zhao, "Fast hybrid FEM/CRE-UTD method to compute the radiation pattern of antennas on large carriers," *Progress In Electromagnetics Research*, PIER 89, 75–84, 2009.
4. Chou, H.-T. and H.-T. Hsu, "Hybridization of simulation codes based on numerical high and low frequency techniques for the efficient antenna design in the presence of electrically large and complex structures," *Progress In Electromagnetics Research*, PIER 78, 173–187, 2008.
5. Chen, M., X.-W. Zhao, and C.-H. Liang, "Analysis of antenna around NURBS surface with iterative MOM-PO technique," *Journal of Electromagnetic Waves and Applications*, Vol. 20, No. 12, 1667–1680, 2006.
6. Lei, J.-Z., C.-H. Liang, W. Ding, and Y. Zhang, "Analysis of airborne phased-array antennas using hybrid method of parallel FDTD and UTD," *Chinese Journal of Radio Science*, Vol. 24, No. 1, 2009.
7. Wang, M., C.-H. Liang, and Y. Zhang, "Combining UTD with MM for pattern prediction of the antenna in complex environment," *Chinese Journal of Radio Science*, Vol. 22, No. 3, 508–512, 2007.
8. Zhang, Y., X.-W. Zhao, M. Chen, and C.-H. Liang, "An efficient MPI virtual topology based parallel, iterative MOM-PO hybrid method on PC clusters," *Journal of Electromagnetic Waves and Applications*, Vol. 20, No. 5, 661–676, 2006.
9. HOBIES user manual, OHRN Enterprises, Inc., Syracuse, New York, 2006, http://lcs.syr.edu/faculty/sarkar/softw.asp#hobies.
10. Zhang, Y. and T. K. Sarkar, *Parallel Solution of Integral Equation*

Based EM Problems in the Frequency Domain, Wiley-IEEE Press, 2009.

11. Zhang, Y., M. Taylor, T. Sarkar, H. Moon, and M. Yuan, "Solving large complex problems using a higher-order basis: Parallel in-core and out-of-core integral-equation solvers," *IEEE Antennas and Propagation Magazine*, Vol. 50, No. 4, 1–30, Aug. 2008.
12. Zhao, X. W. and C.-H. Liang, "Performance comparison between two commercial EM software using higher order and piecewise RWG basis functions," *Microwave Opt. Technol. Lett.*, Vol. 51, 1219–1225, 2009.
13. Kouyoumjian, R. G. and P. H. Pathak, "A uniform geometrical theory of diffraction for an edge in a perfectly-conducting surface," *Proc. IEEE*, Vol. 62, 1448–1461, 1974.
14. Pathak, P. H., W. D. Burnside, and R. J. Marheflca, "A uniform GTD analysis of the diffraction of electromagnetic waves by a smooth convex surface," *IEEE Trans. Antennas Propagat.*, Vol. 28, No. 5, 631–642, Sep. 1980.
15. Branko, M. K., "Electromagnetic modeling of composite metallic and dielectric structures," *IEEE Trans. Microwave Theory and Techniques*, Vol. 47, No. 7, Jul. 1999.
16. Chou, H.-T. and H.-K. Ho, "Implementation of a forward-backward procedure for the fast analysis of electromagnetic radiation/scattering from two-dimensional large phased arrays," *IEEE Trans. Antennas Propagat.*, Vol. 52, No. 2, 388–396, 2004.